ACS OMEGA

http://pubs.acs.org/journal/acsodf

Article

Effect of Rapid Thermal Annealing on Si-Based Dielectric Films Grown by ICP-CVD

Irina Parkhomenko, Liudmila Vlasukova, Fadei Komarov, Nataliya Kovalchuk, Sergey Demidovich, Ainur Zhussupbekova,* Kuanysh Zhussupbekov, Igor V. Shvets, Oleg Milchanin, Dmitry Zhigulin, and Ivan Romanov

Cite This: *ACS Omega* 2023, 8, 30768−30775

Read Online

ACCESS | Metrics & More | Article Recommendations | Supporting Information

ABSTRACT: Silicon nitride, silicon oxide, and silicon oxynitride thin films were deposited on the Si substrate by inductively coupled plasma chemical vapor deposition and annealed at 1100 °C for 3 min in an Ar environment. Silicon nitride and silicon oxide films deposited at ratios of the reactant flow rates of SiH_4/N_2 = 1.875 and SiH_4/N_2O = 3, respectively, were Si-rich, while Si excess for the oxynitride film ($SiH_4/N_2/N_2O$ = 3:2:2) was not found. Annealing resulted in a thickness decrease and structural transformation for SiO_x and SiN_x films. Nanocrystalline phases of Si as well as α- and β-Si_3N_4 were found in the annealed silicon nitride film. Compared to oxide and nitride films, the oxynitride film is the least susceptible to change during annealing. The relationship between the structure, composition, and optical properties of the Si-based films has been revealed. It has been shown that the calculated optical parameters (refractive index, extinction coefficient) reflect structural peculiarities of the as-deposited and annealed films.

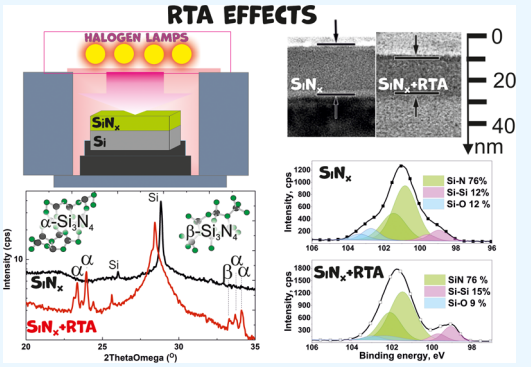

1. INTRODUCTION

Despite all the talk of the end of the silicon era, the Si-based semiconductor industry will continue to satisfy the needs of the market. Recently, much attention has been paid to silicon-based dielectrics such as SiO_x, SiN_x, and SiO_xN_y. Even more, silicon nitride and oxynitride are considered alternative dielectric platforms for integrated photonics.[1−3]

Nowadays, the progress of electronics is related to further miniaturization of chip technology. On-chip capacitor miniaturization requires a thickness decrease of basic dielectric layers such as silicon oxide and nitride films. In addition, there is a tendency to use layered structures and superlattices containing such thin dielectric films.[4−7] Thin films of silicon nitride and oxide enriched with silicon are in the focus of interest today due to the possibility of using them as storage medium for resistive random-access memory (RRAM).[8−12] To obtain the RRAM device with reliable and reproducible resistive switching characteristics, the thickness, chemical, and phase composition of storage medium—Si-based dielectric layer—should be strictly controlled. Unfortunately, control and diagnostics of ultrathin Si-based dielectric layers are getting dramatically more complicated.

In this work, we investigated thin dielectric films of Si-enriched silicon oxide and nitride as well as silicon oxynitride obtained by inductively coupled plasma chemical vapor deposition (ICP-CVD). This low-temperature method allows us to deposit uniform large-area films with a low level of radiative defects, which is crucial for modern technologies including conformable electronics.[13] To the best of our knowledge, Si-based ICP-CVD films have not been studied in detail, especially oxide and oxynitride ones. Also, the effect of rapid thermal annealing of ICP-CVD Si-based films is scarcely represented in the published literature. Besides, the ICP-CVD films with a thickness of more than 60 nm were mostly discussed in published articles.[13−16] The thickness of the films discussed in the present work is about 10−25 nm. Diagnostics of such thin films is more complicated, yet necessary, as the role of interface effects during deposition and subsequent annealing increases with decreasing thickness.[17] The aim of our study was to reveal the relationship between the structure and composition and the optical properties of the Si-based films, all immensely important for the future design of optoelectronic and photonic systems based on such films.

2. EXPERIMENTAL SECTION

Silicon nitride, oxide, and oxynitride films were deposited on p-type silicon substrates ⟨111⟩ (100 mm in diameter) by ICP-

Received: July 12, 2023
Accepted: July 28, 2023
Published: August 8, 2023

Table 1. Deposition Regimes of Si-Based Dielectric Films

sample	SiH_4 (sccm)	N_2 (sccm)	N_2O (sccm)	Ar (sccm)	He (sccm)	p (Pa)	ICP power (W)	t (s)	r (nm/min)
SiN_x	15	8		75	120	2.5	1000	37	39.6
SiO_x	15		5	10	120	1.8	800	12	58.5
SiO_xN_y	15	10	10	40	120	2.0	1000	41	34.4

CVD using a STE ICP200D system (SemiTEq). The initial silicon substrates were treated in Caro's acid and ammonia peroxide mixture and further cleaned in Ar in the reactor at an ICP source power of 300 W for 120 s at 105 °C. The deposition temperature in all cases was 300 °C, and the RF discharge power was in the range of (800−1000) W. The flow rate of reagent gases, chamber pressure, deposition time (t), and deposition rate (r) are given in Table 1. The flow rate of monosilane (SiH_4) remained the same for all deposition processes. Nitrogen (N_2) and nitrous oxide (N_2O) were used as reactant gases for the deposition of SiN_x and SiO_x, respectively. In the case of SiO_xN_y, both these gases mixed in equal proportions were utilized. An Ar + He mixture was used as a carrier gas.

Then, the 1 × 1 cm^2 samples were cut out from wafers with deposited dielectric films, placed on a silicon substrate, and annealed at 1100 °C for 3 min in an Ar atmosphere using a rapid thermal annealing (RTA) furnace (AS-Master, Annealsys, France) with a heating rate of 70 °C/s.

The thicknesses of layers were measured by scanning electron microscopy (SEM) using a Hitachi S-4800 microscope and by transmission electron microscopy (TEM) in a cross-sectional technique using a Hitachi H-800 microscope operated at 200 keV. Additionally, TEM images in a plan-view technique and selected area electron diffraction (SAED) patterns were taken.

The crystal structure and compositional analyses of the ultrathin films were performed via X-ray diffraction (XRD) and X-ray photoelectron spectroscopy (XPS), respectively. The elemental composition was measured by XPS in an Omicron MultiProbe XPS instrument (Scienta Omicron Inc., Uppsala, Sweden). High-resolution spectra were obtained at 20 eV pass energy using a monochromatic X-ray source. The obtained spectra were analyzed using CasaXPS software with fitting of the Gauss−Lorentz form and the Shirley background. All energy positions are corrected for C 1s (284.8 eV). Photoelectronic spectra of Si 2p levels were fitted by three components (Si−N, Si−O, elemental Si). Each component was adjusted taking into account the contributions of Si $2p_{3/2}$ and Si $2p_{1/2}$[18] and the spin−orbit splitting of 0.63 eV, usually employed for elemental Si. XRD measurements were performed on an X-ray diffractometer (Bruker d8 Advance) using a un-monochromated Cu Kα radiation (wavelength of 1.54 Å) at 40 kV and 40 mA through a 0.6 mm slit at an angle of (10−70°).

The optical properties were investigated through measurements of the specular reflectance spectra at 8° incident angle using the universal reflectance accessory of a LAMBDA-1050 ultraviolet−visible−near-infrared(UV−vis−NIR) spectrophotometer in the range of 190−1000 nm with an accuracy of 0.1%. RefFit Software[19] was used to fit the reflectance spectra and to extract optical parameters (refractive index, extinction and absorption coefficient, energy band gap).

3. RESULTS AND DISCUSSION

3.1. SEM and TEM. In order to obtain reliable information from optical spectra (refractive index, extinction coefficient), it is necessary to know the exact value of the film thickness. In this work, the thickness of the as-deposited films was initially determined by ellipsometry. However, this method can give erroneous results for nonstoichiometric films. Therefore, the film thickness was additionally estimated by SEM and TEM. The results of thickness measurements by various methods are shown in Table 2. For greater clarity, the cross-sectional SEM images of the samples with dielectric films are shown in Figure 1a. The corresponding TEM images are shown in Figure S1 of the SI.

Table 2. Thickness of Si-Based Dielectric Films

sample	ellipsometry d (nm)	SEM d (nm)	TEM d (nm)
SiN_x	24.4	23.8 ± 1	24.6 ± 2
SiN_x after RTA		19.8 ± 1	18.4 ± 0.5
SiO_x	11.7	10.6 ± 1	11.9 ± 1.0
SiO_x after RTA		7.9 ± 1	7.5 ± 0.5
SiO_xN_y	23.5	25.1 ± 1	26.9 ± 1.0
SiO_xN_y after RTA		25.1 ± 1	28.8 ± 1.0

As can be seen from Table 2, a good correlation is observed between the values of thicknesses obtained by different methods. Besides, SEM and TEM data reveal the thickness decrease for the SiN_x and SiO_x films after thermal treatment. Probably, this is due to the film densification and the increase in residual stress after annealing.[20] In the case of SiO_xN_y, SEM data have not changed, while TEM data show a slight increase of thickness. The absence of the film shrinkage indicates the suppression of increasing residual stress during the heat treatment.

Figure 1b,c shows the cross-sectional and dark-field plan-view TEM images of the annealed SiN_x film, respectively. The dark-field TEM image displays small inclusions of light contrast, which indicates the presence of crystalline nanoclusters. Unfortunately, the SAED reflections from the silicon substrate suppress the weak signal from the nanocrystals.

3.2. XRD. Figure 2 depicts the XRD spectra of the samples. A peak at around 28.5° is observed in all spectra. This peak is attributed to the Si crystal facets of (111) and is due to the substrate contribution.[21,22] However, in the case of the sample with the as-deposited SiN_x, a shift of this peak position to 28.8° is observed. It can indicate a tensile strain of Si. We suppose that it is due to formation of the surface transition silicon layer at the initial step of deposition. Afterward, this transition layer crystallized and cooled testing tensile stress under the top SiN_x layer. The similar effect of the thin capping layer on residual stress underlying silicon is described in refs 23, 24. The wide band at 20−22° corresponding to the amorphous phase should be also noted, presumably SiO_x.[25,26] RTA eliminates the "tensile strain" shift and "amorphous" band. Besides, RTA results in broadening of the (111) peak as well as formation of a narrow peak set. These narrow peaks indicate the formation

https://doi.org/10.1021/acsomega.3c04997
ACS Omega 2023, 8, 30768−30775

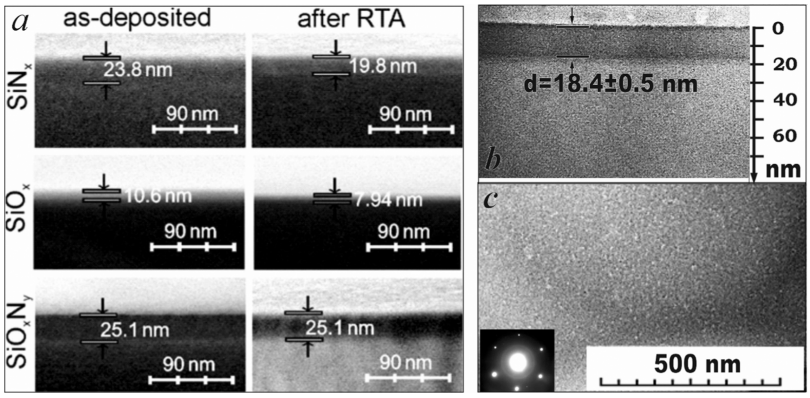

Figure 1. Cross-sectional SEM images of the SiN_x, SiO_x, and SiO_xN_y films before and after RTA (a) and cross-sectional (b) and dark-field plan-view (c) TEM images of the SiN_x film after RTA. The inset shows the corresponding SAED pattern.

of Si nanocrystals[27−29] and nanocrystalline phases, α- and β-Si_3N_4.[22] Formation of such phases occurs at normal pressure yet at high temperature.[30] However, these requirements for nanocrystals can be relaxed.[31] For example, α-Si_3N_4 nanocrystals were registered in silicon oxynitride films deposited using ICP-CVD.[14] The multilayered plasma-enhanced CVD-SiN_x film contained α- and β-Si_3N_4 nanocrystals after annealing at 1100−1150 °C.[22,31] Moreover, the 2 × 2 silicon (111) unit cell has a lattice mismatch of only about 1.1% with the "*a*" axis of hexagonal Si_3N_4.[32] Therefore, the orientation of the Si substrate (111) in our case favors the formation of the silicon nitride crystalline phase. Thus, we can conclude that clusters with light contrast observed in the TEM image (Figure 1c) are Si and Si_3N_4 nanocrystals.

The effect of RTA on the crystal structure is less expressed for the silicon oxide film. In the case of the as-deposited SiO_x film, the Si (111) band is wider than for the as-deposited silicon nitride. This broadening can be related to the amorphous silicon or silicon oxide phase. RTA results in this band narrowing that indicates crystallization of the amorphous Si phase and/or ordering of the SiO network. The as-deposited silicon oxynitride sample also demonstrates broadening of the (111) band in comparison with the SiN_x one; however, RTA does not result in noticeable changes.

3.3. XPS. The atomic concentrations of the elements Si, C, N, and O for the SiN_x, SiO_x, and SiO_xN_y films calculated from XPS data are shown in Table 3. Taking into account the stoichiometric ratio for silicon nitride ([N]/[Si] = 1.3) and silicon oxide ([O]/[Si] = 2), the as-deposited SiN_x and SiO_x films are Si-rich ones. The Si excess is 34 and 57% for SiN_x and SiO_x, respectively. In the case of silicon oxynitride films, the ratio [O]/([O] + [N]) was calculated. The value of this parameter below/above 0.4 indicates a nitride-like/oxide-like structure.[33] In our case, the as-deposited SiO_xN_y film exhibits a ratio of 0.6 that suggests an oxide-like structure. RTA results in the decrease of carbon contamination for all films. In the case of SiN_x and SiO_xN_y, the oxygen concentration increases, while for the SiO_x film, the nitrogen concentration increases after RTA.

Let us briefly discuss the presence of hydrogen in the films under investigation. We failed to register the signal from hydrogen or Si−H and N−H bonds by XPS as well as by IR spectroscopy (not shown here). Possibly, the films in our experiment are too thin, and the H-signal is below the detection limit of using techniques. Nevertheless, we are inclined toward the low hydrogen concentration in the as-deposited dielectric films. First, ICP-CVD films are characterized as a low H content due to the used high-density plasma and N_2 as a precursor instead of NH_3.[34,35] Second, one needs to consider the relatively high chosen value of deposition temperature and ICP power, which stimulates a reduction of H the content.[36]

Figure 3 shows the XPS spectra of the as-deposited and annealed Si-based dielectrics.

Quantitative analysis was carried out using the Si 2p core level. The range at 98−105 eV displays Si 2p peaks deconvoluted to Si^{4+}, Si^{3+}, Si^{2+}, and Si^{1+} components related to dioxide and nitride phases and suboxide phases.[37,38] The obtained results are presented in the insets in Figure 3. The XPS spectrum of the as-deposited SiN_x film displays components assigned to silicon oxide, silicon nitride, and elemental silicon. The broad peaks imply a variation in atomic arrangements surrounding the bonds. Annealing results in a decrease of the contribution from Si−O bonds. The bands related to Si−N and Si−Si bonds become narrower and more defined, indicating the increase in the crystallization degree. It agrees with the XRD data on a decrease of contribution from the amorphous silicon oxide phase and about Si and Si_3N_4 nanocrystal formation.

Broad peaks related to Si−O and Si−Si bonds are manifested in the spectrum of the as-deposited SiO_x film. RTA leads to narrowing of Si−O and increase of Si−Si components, as in the case of SiN_x. A comparison of SiO_x and SiN_x samples reveals a higher percentage increase of the Si−Si band for SiO_x films (by 14%). One can suggest that a formation of Si nanocrystals in the SiO_x matrix during RTA proceeds more actively due to the higher Si excess in the as-deposited film. The absence of separate Si peaks in the XRD spectrum of the annealed SiO_x sample, which were registered for SiN_x, can be explained by the thinner (at least 2 times) film.

The XPS spectrum of the as-deposited oxynitride exhibits only bands related to Si−O and Si−N bonds and no bands from Si−Si bonds. Compared to oxide and nitride films, the oxynitride film is the least susceptible to change during RTA.

3.4. Optical Properties. Figure 4 shows the reflectance spectra of the as-deposited and annealed films. The as-deposited SiN_x film demonstrates reflectance minimum R = 0.087% at 290 nm. Such a low value of reflectance suggests that the refractive index of the SiN_x film corresponds to almost perfect antireflection coating (square root of the substrate's refractive index). RTA results in fading of the antireflection effect (R = 6.85%). In the case of the SiO_x film, annealing also

https://doi.org/10.1021/acsomega.3c04997
ACS Omega 2023, 8, 30768−30775

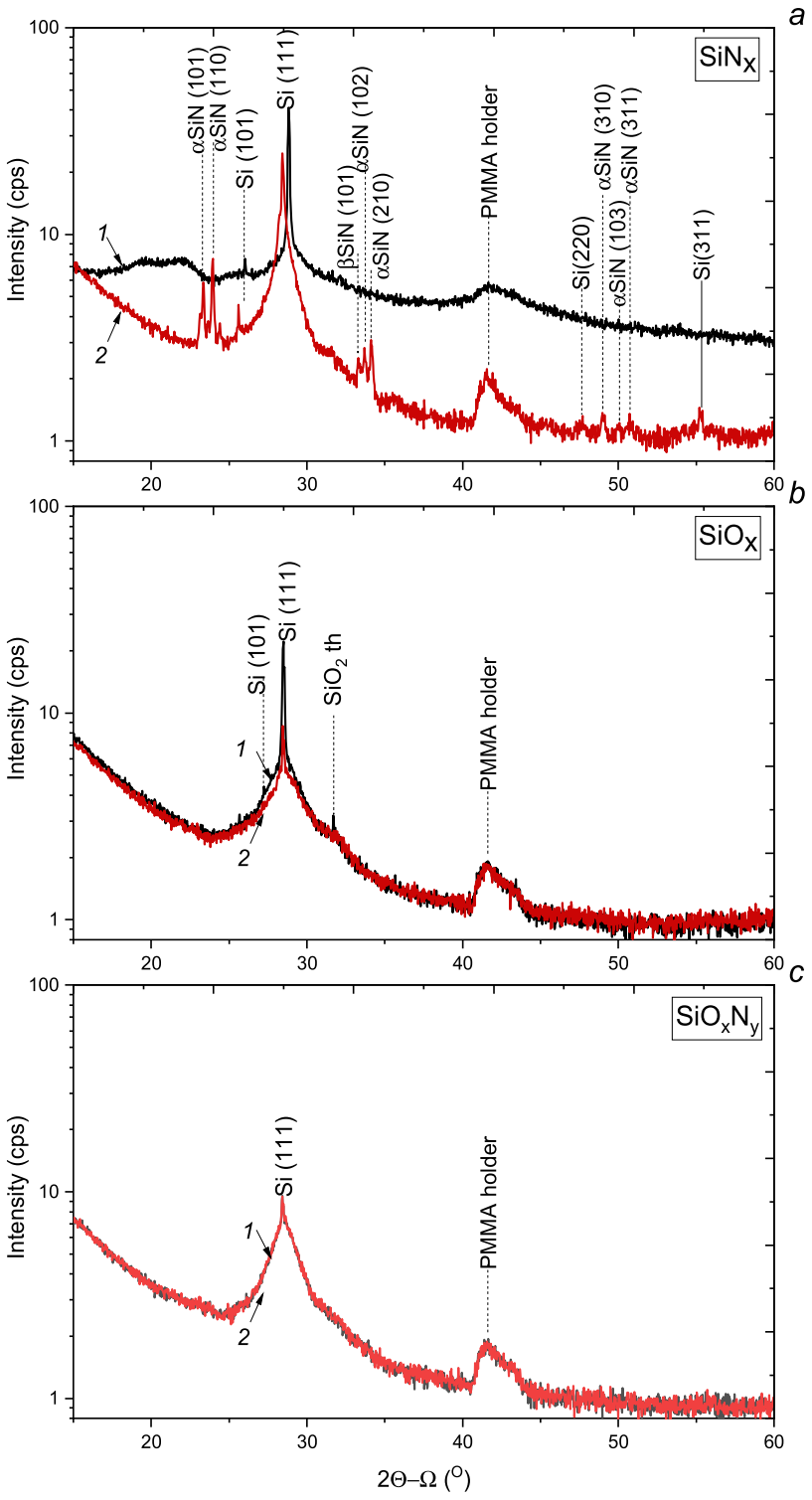

Figure 2. XRD spectra of the SiN_x (a), SiO_x (b), and SiO_xN_y (c) films before (1) and after RTA (2).

leads to the increase of reflectance by ∼10−20% in the range of 200−400 nm. The same trend, yet to a lesser extent, is observed for oxynitride films.

Figure 5 shows the corresponding refractive index n and extinction coefficient k as functions of wavelength obtained using RefFit software. The refractive index of the SiN_x film is about 2.0−2.1 in the VIS range, typical for the CVD SiN_x film.[15,39] However, the refractive index spectrum of the as-deposited SiN_x exhibits a maximum at 220 nm, and the extinction coefficient is rather high (0.05−0.015 in VIS). It is typical for Si-rich films.[40,41] RTA results in an increase of n and k in the visible spectral range and a red-shifted maximum in the UV range. The red shift is closely related to an optical band gap decrease. According to our estimates using Tauc's plots (Figure S2 in SI), the optical band gap decreases from 3.5 to 2.4 eV after RTA.

The refractive index and extinction coefficient of the SiO_x film is also quite high, $n \sim 1.6$ and $k \sim 0.07$−0.23 in the VIS

https://doi.org/10.1021/acsomega.3c04997
ACS Omega 2023, 8, 30768−30775

Table 3. Atomic concentration (atom %) of Si, N, C, and O Elements of Si-Based Dielectric Films

sample	Si	N	O	C	atomic ratio
SiN_x	51.4	17.0	12.8	21.6	[N]/[Si]~0.3
SiN_x after RTA	50.5	20.8	16.4	13.3	[N]/[Si]~0.4
SiO_x	55.7	7.7	22.0	26.0	[O]/[Si]~0.4
SiO_x after RTA	44.9	12.4	22.3	10.2	[O]/[Si]~0.5
SiO_xN_y	56.4	14.9	26.9	14.6	[O]/[O + N]~0.6
SiO_xN_y after RTA	54.05	12.45	28.1	13.5	[O]/[O + N]~0.7

range, respectively. It indicates a high Si content in the film or/and high level of structural disordering[42] that agrees with XPS data. As in the case of SiN_x, RTA results in the refractive index increase with an appearance of a maximum at 385 nm and in a substantial increase of the extinction coefficient up to 1.5 at 310 nm. It additionally proves the synthesis of Si nanocrystals in the silica matrix.

The silicon oxynitride film exhibits the refractive index n = 2.05−2.15 in the VIS range that is close to n for silicon nitride. It can assume a low concentration of oxygen in the oxynitride film.[43] The extinction coefficient ($k \sim 0.05-0.1$) is the lowest among the discussed dielectrics. The obtained values of n and k are less than the ones for the Si-rich silicon oxynitride deposited by magnetron sputtering in ref 44 that additionally confirmed the absence of Si excess in the deposited film. Ref 45 reports the results of the study of SiN_xO_y thin films deposited under different conditions at room temperature by plasma-enhanced CVD. The authors studied the chemical composition of SiN_xO_y films by FTIR spectroscopy and presented the N/Si ratio as a function of the refractive index. In our experiment, the silicon oxynitride film is characterized with n = 2.05−2.15. According to ref 45, this corresponds to the N/Si ratio ≈ 1.3. The values of n and k for SiO_xN_y remain virtually unchanged after RTA, which additionally confirms the stability of the film's structure.

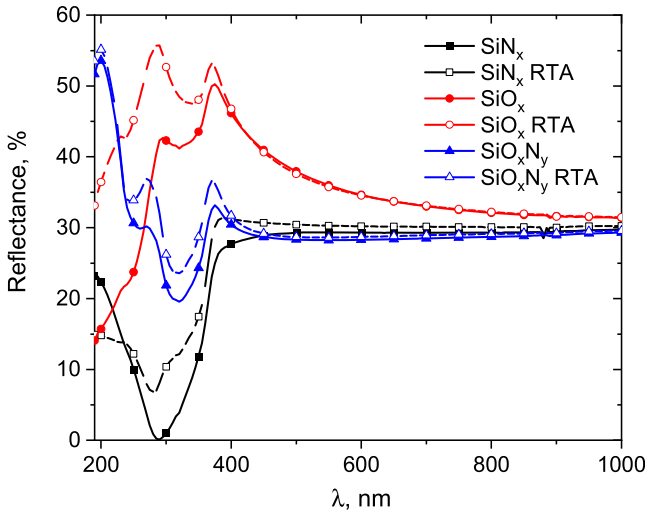

Figure 4. Reflectance spectra of the SiN_x, SiO_x, and SiO_xN_y films before and after RTA.

The similar behavior of optical constants for SiN_x and SiO_x films after annealing can be explained by the formation of Si-rich films with the disordering structure due to a relatively large flow rate of SiH_4. Further annealing stimulates some structure transformation, namely atomic rearrangement of the host matrix as well as formation of nanocrystals. Such processes appear to be responsible for shrinking thicknesses for SiN_x and SiO_x films. In the case of silicon oxynitride, the flow rate of SiH_4 is the same as for deposition of SiN_x and SiO_x. However, SiH_4 molecules could interact with N_2 as well as with N_2O, and the Si excess in the deposited oxynitride film is minor. This favors the formation of a homogeneous structure resistant to high temperatures.

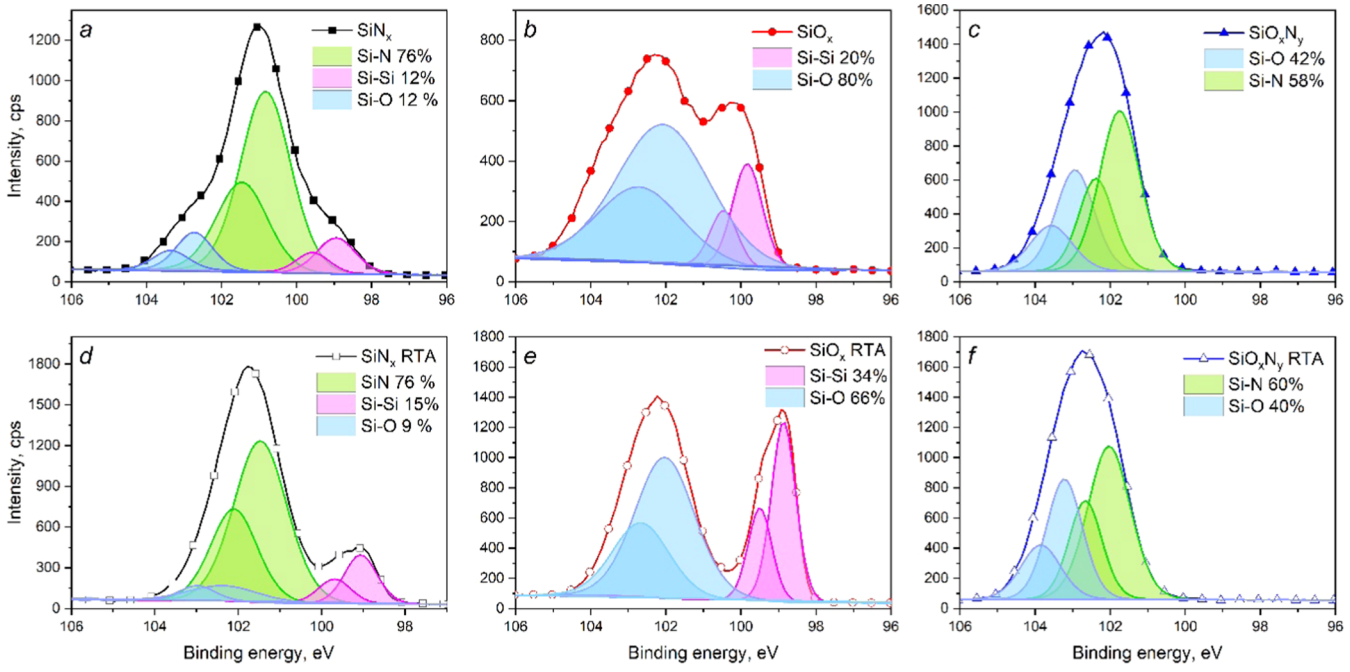

Figure 3. Si 2p XPS spectra of the SiN_x (a, d), SiO_x (b, e), and SiO_xN_y (c, f) films before (a−c) and after RTA (d−f).

https://doi.org/10.1021/acsomega.3c04997
ACS Omega 2023, 8, 30768−30775

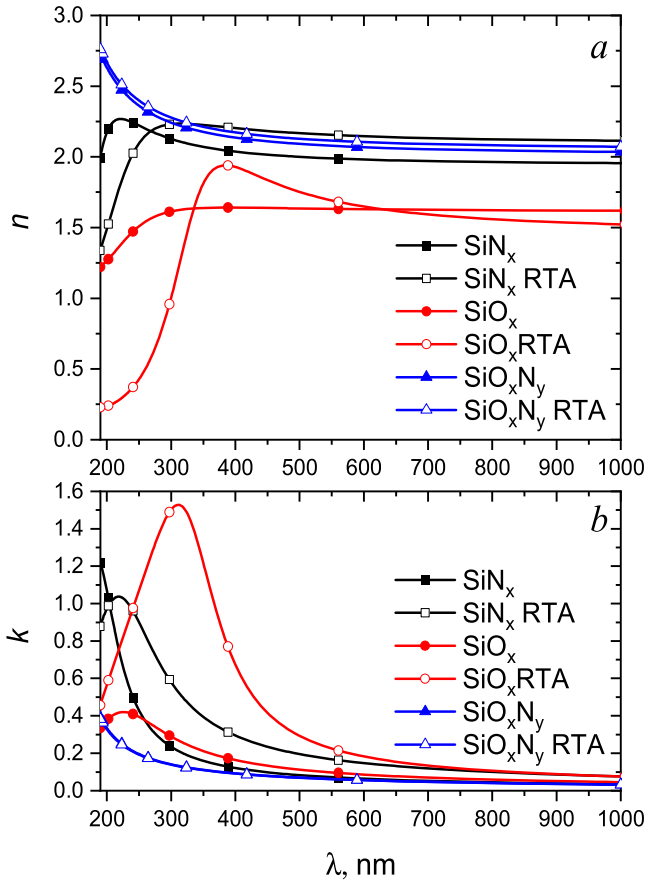

Figure 5. Dispersion of refractive index (a) and extinction coefficient (b) of the SiN_x, SiO_x, and SiO_xN_y films before and after RTA.

4. CONCLUSIONS

Silicon oxide, nitride, and oxynitride films with the thickness of 10−25 nm were synthesized by ICP-CVD at the fixed SiH_4 flow rate. The other reactants of the deposition process were N_2, N_2O, and N_2 + N_2O for SiN_x, SiO_x, and SiO_xN_y, respectively. After that, the samples went through RTA at 1100 °C for 3 min. Practically important results are that RTA leads to a decrease of thickness for silicon oxide and nitride films, while the thickness of the silicon oxynitride film remains unchanged. We suggest that this is due to an excess content of Si and a disorder in the as-deposited SiN_x and SiO_x films, while the as-deposited SiO_xN_y has an initially more ordered structure without substantial Si excess. The rapid thermal annealing initiates structural transformation for SiN_x and SiO_x films, namely, recovery structure of the host matrix and formation of Si nanocrystals. Moreover, formation of α- and β-Si_3N_4 nanocrystals in the case of the SiN_x film was revealed by XRD.

It has been shown that optical parameters (refractive index n and extinction coefficient k) reflect structural peculiarities of the as-deposited and annealed films. In the case of SiN_x and SiO_x, RTA results in an increase of n and k in the VIS range as well as the maximum red shift in the UV range, which is typical for Si-rich films and indicates formation of Si nanocrystals in the dielectric matrix. The intensity of n and k maxima is higher in the spectra of SiO_x samples. Hence, we can conclude that Si nanocrystal formation in the SiO_x matrix proceeds more actively than in silicon nitride. It agrees with the XPS data. The revealed regularities can be useful in choosing Si-based dielectrics for electro-optics and MEMS devices. Also, formation of the crystalline silicon nitride film on the Si substrate can ensure the sustainability of crystalline growth of III nitrides materials (GaN, AlN) on silicon.

■ ASSOCIATED CONTENT

Supporting Information

The Supporting Information is available free of charge at https://pubs.acs.org/doi/10.1021/acsomega.3c04997.

Additional cross-sectional TEM images of the SiN_x, SiO_x, and SiO_xN_y films as well as Tauc's plot of SiN_x before and after RTA is included (PDF)

■ AUTHOR INFORMATION

Corresponding Author

Ainur Zhussupbekova − *School of Physics and Centre for Research on Adaptive Nanostructures and Nanodevices (CRANN), Trinity College Dublin, Dublin D02 PN40, Ireland; L.N. Gumilyov Eurasian National University, Astana 010000, Kazakhstan;* orcid.org/0000-0003-2724-8762; Email: zhussupa@tcd.ie

Authors

Irina Parkhomenko − *Belarusian State University, 220045 Minsk, Belarus;* orcid.org/0000-0003-0982-3938

Liudmila Vlasukova − *Belarusian State University, 220045 Minsk, Belarus*

Fadei Komarov − *A.N. Sevchenko Institute of Applied Physical Problems of Belarusian State University, 220045 Minsk, Belarus*

Nataliya Kovalchuk − *Joint Stock Company "Integral", 220108 Minsk, Belarus*

Sergey Demidovich − *Joint Stock Company "Integral", 220108 Minsk, Belarus*

Kuanysh Zhussupbekov − *School of Physics and Centre for Research on Adaptive Nanostructures and Nanodevices (CRANN), Trinity College Dublin, Dublin D02 PN40, Ireland;* orcid.org/0000-0003-1909-3270

Igor V. Shvets − *School of Physics and Centre for Research on Adaptive Nanostructures and Nanodevices (CRANN), Trinity College Dublin, Dublin D02 PN40, Ireland*

Oleg Milchanin − *A.N. Sevchenko Institute of Applied Physical Problems of Belarusian State University, 220045 Minsk, Belarus*

Dmitry Zhigulin − *Joint Stock Company "Integral", 220108 Minsk, Belarus*

Ivan Romanov − *Belarusian State University, 220045 Minsk, Belarus*

Complete contact information is available at: https://pubs.acs.org/10.1021/acsomega.3c04997

Author Contributions

All authors contributed equally. The article was written through contributions of all authors. All authors have given approval to the final version of the article.

Funding

This study was supported by the Belarusian state program of scientific research Photonics and electronic for innovations (projects 3.8.1, SR No 20212595).

Notes

The authors declare no competing financial interest.

■ ACKNOWLEDGMENTS

A.Z. would like to acknowledge funding from the Ministry of Science and Higher Education of the Republic of Kazakhstan (Grant No. AP19175233) and the Irish Research Council through Award No. GOIPD/2022/443. This paper concerns work carried out from 2019 to 2021.

■ ABBREVIATIONS

RRAM, resistive random-access memory; ICP-CVD, inductively coupled plasma chemical vapor deposition; RTA, rapid thermal annealing; SEM, scanning electron microscopy; TEM, transmission electron microscopy; SAED, selected area electron diffraction; XPS, X-ray photoelectron spectroscopy

■ REFERENCES

(1) Blumenthal, D. J.; Heideman, R.; Geuzebroek, D.; Leinse, A.; Roeloffzen, C. Silicon Nitride in Silicon Photonics. *Proc. IEEE* **2018**, *106*, 2209−2231.
(2) Piccoli, G.; Sanna, M.; Borghi, M.; Pavesi, L.; Ghulinyan, M. Silicon Oxynitride Platform for Linear and Nonlinear Photonics at NIR Wavelengths. *Opt. Mater. Express* **2022**, *12*, 3551−3662.
(3) Ng, D. K. T.; Wang, Q.; Wang, T.; Ng, S.-K.; Toh, Y.-T.; Lim, K.-P.; Yang, Y.; Tan, D. T. H. Exploring High Refractive Index Silicon-Rich Nitride Films by Low-Temperature Inductively Coupled Plasma Chemical Vapor Deposition and Applications for Integrated Waveguides. *ACS Appl. Mater. Interfaces* **2015**, *7*, 21884−21889.
(4) Avilés-Bravo, J. J.; Palacios-Huerta, L.; Aceves-Mijares, M.; González-Flores, K. E.; Morales-Morales, F.; Morales-Sánchez, A. Impact of the Gate Fabrication Process of Light Emitting Capacitors Based on Silicon-Rich Oxide: Low Voltage Electroluminescence. *J. Lumin.* **2021**, *240*, No. 118470.
(5) Yang, Y.; Liu, Y.; Yang, S.; Wu, Y.; Tian, H. Double-Layered Silicon-Nitride Photonic Crystal Slab Guided-Mode-Resonance High-Sensitivity Sensor Application for Refractive Index Sensing and Nanoparticle Detection. *J. Opt. Soc. Am. B* **2021**, *38*, 1927−1933.
(6) Michailovska, K.; Dan'ko, V.; Indutnyi, I.; Shepeliavyi, P.; Sopinskyy, M. Polarized Luminescence of Silicon Nanoparticles Formed in (SiOx−SiOy)n Superlattice. *Appl. Nanosci.* **2022**, *12*, 479−488.
(7) Ma, H.-P.; Gu, L.; Shen, Y.; Huang, W.; Liu, Y.-H.; Zhu, J.-T.; Zhang, Q.-C. Annealing Effect on SiNx/SiO2 Superlattice with Ultrathin Sublayer Fabricated Using Plasma-Enhanced Atomic Layer Deposition. *Ceram. Int.* **2022**, *48*, 22123−22130.
(8) Gismatulin, A. A.; Gritsenko, V. A.; Yen, T.-J.; Chin, A. Charge Transport Mechanism in SiN x -Based Memristor. *Appl. Phys. Lett.* **2019**, *115*, No. 253502.
(9) Lu, Y.; Alvarez, A.; Kao, C.-H.; Bow, J.-S.; Chen, S.-Y.; Chen, I.-W. An Electronic Silicon-Based Memristor with a High Switching Uniformity. *Nat. Electron.* **2019**, *2*, 66−74.
(10) Yen, T. J.; Chin, A.; Gritsenko, V. High Performance All Nonmetal SiNx Resistive Random Access Memory with Strong Process Dependence. *Sci. Rep.* **2020**, *10*, No. 2807.
(11) Lee, Y.; Shin, J.; Nam, G.; Chung, D.; Kim, S.; Jeon, J.; Kim, S. Atomic Layer Deposited SiOx-Based Resistive Switching Memory for Multi-Level Cell Storage. *Metals* **2022**, *12*, No. 1370.
(12) Sun, B.; Han, X.; Xu, R.; Qian, K. Uncovering the Indium Filament Formation and Dissolution in Transparent ITO/SiN x /ITO Resistive Random Access Memory. *ACS Appl. Electron. Mater.* **2020**, *2*, 1603−1608.
(13) Yang, K.; De Sagazan, O.; Pichon, L.; Salaün, A.-C.; Coulon, N. Inductively Coupled Plasma Chemical Vapor Deposition for Silicon-Based Technology Compatible with Low-Temperature (≤220 °C) Flexible Substrates. *Phys. Status Solidi (a)* **2020**, *217*, No. 1900556.
(14) Fainer, N. I.; Kosinova, M. L.; Maximovsky, E. A.; Rumyantsev, Y. M.; Kuznetsov, F. A.; Kesler, V. G.; Kirienko, V. V. Study of the Structure and Phase Composition of Nanocrystalline Silicon Oxynitride Films Synthesized by ICP-CVD. *Nucl. Instrum. Methods Phys. Res., Sect. A* **2005**, *543*, 134−138.
(15) Kshirsagar, A.; Nyaupane, P.; Bodas, D.; Duttagupta, S. P.; Gangal, S. A. Deposition and Characterization of Low Temperature Silicon Nitride Films Deposited by Inductively Coupled Plasma CVD. *Appl. Surf. Sci.* **2011**, *257*, 5052−5058.
(16) Luna-Sánchez, R. M.; González-Martínez, I. The Low Leakage Current Density of MIS with SiO2 Film Made by ICP-CVD. *ECS Trans.* **2006**, *2*, 261−266.
(17) Belyansky, M.; Chace, M.; Gluschenkov, O.; Kempisty, J.; Klymko, N.; Madan, A.; Mallikarjunan, A.; Molis, S.; Ronsheim, P.; Wang, Y.; Yang, D.; Li, Y. Methods of Producing Plasma Enhanced Chemical Vapor Deposition Silicon Nitride Thin Films with High Compressive and Tensile Stress. *J. Vac. Sci. Technol., A* **2008**, *26*, 517−521.
(18) Silicon. Silicon X-ray photoelectron spectra, silicon electron configuration, and other elemental information. https://www.thermofisher.com/ie/en/home/materials-science/learning-center/periodic-table/metalloid/silicon.html.
(19) Kuzmenko, A. B. Kramers−Kronig Constrained Variational Analysis of Optical Spectra. *Rev. Sci. Instrum.* **2005**, *76*, No. 083108.
(20) Jiang, W.; Xu, D.; Xiong, B.; Wang, Y. Effects of Rapid Thermal Annealing on LPCVD Silicon Nitride. *Ceram. Int.* **2016**, *42*, 1217−1224.
(21) Chen, J.; Wang, W.; Cherng, J. S.; Chen, Q. High Growth Rate of Microcrystalline Silicon Films Prepared by ICP-CVD with Internal Low Inductance Antennas. *Plasma Sci. Technol.* **2014**, *16*, 502−505.
(22) Scardera, G.; Bellet-Amalric, E.; Bellet, D.; Puzzer, T.; Pink, E.; Conibeer, G. Formation of a Si - Si3 N4 Nanocomposite from Plasma Enhanced Chemical Vapour Deposition Multilayer Structures. *J. Cryst. Growth* **2008**, *310*, 3685−3689.
(23) Park, J.; Kwon, S.; Jun, S.-I.; Ivanov, I. N.; Cao, J.; Musfeldt, J. L.; Rack, P. D. Stress Induced Crystallization of Hydrogenated Amorphous Silicon. *Thin Solid Films* **2009**, *517*, 3222−3226.
(24) Maitrejean, S.; Loubet, N.; Augendre, E.; Morin, P. F.; Reboh, S.; Bernier, N.; Wacquez, R.; Lherron, B.; Bonnevialle, A.; Liu, Q.; Hartmann, J.-M.; He, H.; Halimaoui, A.; Li, J.; Pilorget, S.; Kanyandekwe, J.; Grenouillet, L.; Chafik, F.; Morand, Y.; Le Royer, C.; Faynot, O.; Celik, M.; Doris, B.; de Salvo, B. A New Method to Induce Tensile Stress in Silicon on Insulator Substrate: From Material Analysis to Device Demonstration. *ECS Trans.* **2015**, *66*, 47−56.
(25) Li, M.; Gu, J.; Feng, X.; He, H.; Zeng, C. Amorphous-Silicon@silicon Oxide/Chromium/Carbon as an Anode for Lithium-Ion Batteries with Excellent Cyclic Stability. *Electrochim. Acta* **2015**, *164*, 163−170.
(26) Comedi, D.; Zalloum, O. H. Y.; Irving, E. A.; Wojcik, J.; Roschuk, T.; Flynn, M. J.; Mascher, P. X-Ray-Diffraction Study of Crystalline Si Nanocluster Formation in Annealed Silicon-Rich Silicon Oxides. *J. Appl. Phys.* **2006**, *99*, No. 023518.
(27) Benyahia, B.; Tiour, F.; Guerbous, L.; Chaoui, R.; Menous, I.; Mahmoudi, B.; Mefoued, A.; Guenda, A. Evolution of Optical and Structural Properties of Silicon Nanocrystals Embedded in Silicon Nitride Films with Annealing Temperature. *J. Nano Res.* **2017**, *49*, 163−173.
(28) Das, D.; Patra, C. Wide Optical Gap B-Doped Nc-Si Thin Films with Advanced Crystallinity and Conductivity on Transparent Flexible Substrates for Potential Low-Cost Flexible Electronics Including Nc-Si Superstrate p−i−n Solar Cells. *Mater. Adv.* **2021**, *2*, 2055−2067.
(29) Kharin, A. Y.; Assilbayeva, R. B.; Kargina, Y. V.; Timoshenko, V. Y. Comparative Analysis of Silicon Nanostructures by X-Ray Diffraction Technique. *IOP Conf. Ser. Mater. Sci. Eng.* **2019**, *475*, No. 012010.
(30) Yu, C.-H.; Chiu, K.-A.; Do, T.-H.; Chang, L.; Chen, W.-C. Formation of Aligned α-Si3N4 Microfibers by Plasma Nitridation of Si (110) Substrate Coated with SiO2. *Coatings* **2021**, *11*, No. 1251.
(31) Scardera, G.; Puzzer, T.; Pink, E.; Conibeer, G.; Green, M. A. In *Effect of Annealing Temperature on the Formation of Silicon Nanocrystals in a Nitride Matrix*, Proceedings Volume 6415, Micro-

https://doi.org/10.1021/acsomega.3c04997
ACS Omega 2023, 8, 30768−30775

and Nanotechnology: Materials, Processes, Packaging, and Systems III, Chiao, J.-C.; Dzurak, A. S.; Jagadish, C.; Thiel, D. V., Eds.; SPIE, 2006.
(32) Gangopadhyay, S. Crystalline Silicon Nitride Films on Si(111): Growth Mechanism, Surface Structure and Chemistry down to Atomic Scale. In *Multilayer Thin Films - Versatile Applications for Materials Engineering*; IntechOpen, 2020.
(33) Chen, K.; Lin, Z.; Zhang, P.; Huang, R.; Dong, H.; Huang, X. Luminescence Mechanism in Amorphous Silicon Oxynitride Films: Band Tail Model or N-Si-O Bond Defects Model. *Front. Phys.* **2019**, *7*, No. 144.
(34) Zhou, H.; Elgaid, K.; Wilkinson, C.; Thayne, I. Low-Hydrogen-Content Silicon Nitride Deposited at Room Temperature by Inductively Coupled Plasma Deposition. *Jpn. J. Appl. Phys.* **2006**, *45*, No. 8388.
(35) Huang, X. D.; Gan, X. F.; Zhang, F.; Huang, Q. A.; Yang, J. Z. Improved Electrochemical Performance of Silicon Nitride Film by Hydrogen Incorporation for Lithium-Ion Battery Anode. *Electrochim. Acta* **2018**, *268*, 241−247.
(36) Han, S.; Jun, B.; No, K.; Bae, B. Preparation of a - SiN x Thin Film with Low Hydrogen Content by Inductively Coupled Plasma Enhanced Chemical Vapor Deposition. *J. Electrochem. Soc.* **1998**, *145*, 652−658.
(37) Shimoi, N. Synthesis of Anode Active Material Particles for Lithium-Ion Batteries by Surface Modification via Chemical Vapor Deposition and Their Electrochemical Characteristics. *Adv. Powder Technol.* **2017**, *28*, 2366−2372.
(38) Seo, T.; Park, H.; Jeon, G.; Yun, J.; Park, S.; Seong, S.; Chung, Y. Low-Temperature Fabrication (≤150 °C) of High-Quality Sputtered Silicon Oxide Thin Film with Hydrogen Plasma Treatment. *ACS Appl. Electron. Mater.* **2020**, *2*, 3320−3326.
(39) Lelièvre, J.; Kafle, B.; Saint-Cast, P.; Brunet, P.; Magnan, R.; Hernandez, E.; Pouliquen, S.; Massines, F. Efficient Silicon Nitride SiN $_x$:H Antireflective and Passivation Layers Deposited by Atmospheric Pressure PECVD for Silicon Solar Cells. *Prog. Photovoltaics Res. Appl.* **2019**, *27*, 1007−1019.
(40) Romanov, I. A.; Parkhomenko, I. N.; Vlasukova, L. A.; Komarov, F. F.; Kovalchuk, N. S.; Milchanin, O. V.; Makhavikou, M. A.; Mudryi, A. V.; Zhivulko, V. D.; Lu, H.-L. Blue and Red Light-Emitting Non-Stoichiometric Silicon Nitride-Based Structures. *Proc. Natl. Acad. Sci. Belarus, Phys. Math. Ser.* **2018**, *54*, 360−368.
(41) Malik, P.; Gupta, H.; Ghosh, S.; Srivastava, P. Study of Optical Properties of Single and Double Layered Amorphous Silicon Nitride Films for Photovoltaics Applications. *Silicon* **2022**, DOI: 10.1007/s12633-022-02009-7.
(42) Peña-Rodríguez, O.; Manzano-Santamaría, J.; Olivares, J.; Rivera, A.; Agulló-López, F. Refractive Index Changes in Amorphous SiO2 (Silica) by Swift Ion Irradiation. *Nucl. Instrum. Methods Phys. Res., Sect. B* **2012**, *277*, 126−130.
(43) Chen, W.; Stuckelberger, J.; Wang, W.; Phang, S. P.; Macdonald, D.; Wan, Y.; Yan, D. N-Type Polysilicon Passivating Contacts Using Ultra-Thin PECVD Silicon Oxynitrides as the Interfacial Layer. *Sol. Energy Mater. Sol. Cells* **2021**, *232*, No. 111356.
(44) Hänninen, T.; Schmidt, S.; Jensen, J.; Hultman, L.; Högberg, H. Silicon Oxynitride Films Deposited by Reactive High Power Impulse Magnetron Sputtering Using Nitrous Oxide as a Single-Source Precursor. *J. Vac. Sci. Technol., A* **2015**, *33*, No. 05E121.
(45) Xu, W.; Tang, H.; Zhang, Q.-Y.; Zhou, N.; Shen, Y. Room-Temperature Deposition of Low H-Content SiNx/SiNxOy Thin Films Using a Specially Designed PECVD System. *Surf. Coat. Technol.* **2020**, *402*, No. 126506.

https://doi.org/10.1021/acsomega.3c04997
ACS Omega 2023, 8, 30768−30775